PNAS RESEARCH ARTICLE | BIOPHYSICS AND COMPUTATIONAL BIOLOGY

Agonist activation to open the Gα subunit of the GPCR–G protein precoupled complex defines functional agonist activation of TAS2R5

Moon Young Yang[a,1], Khuong Duy Mac[b,1], Hannah R. Strzelinski[c], Samantha A. Hoffman[c], Donghwa Kim[c], Soo-Kyung Kim[a], Judith Su[d,2], Stephen B. Liggett[c,2], and William A. Goddard III[a,2]

Affiliations are included on p. 7.

Contributed by William A. Goddard III; received May 30, 2024; accepted October 17, 2024; reviewed by Marco De Vivo and Cheng Zhang

G protein-coupled receptors (GPCRs) regulate multiple cellular responses and represent highly successful therapeutic targets. The mechanisms by which agonists activate the G protein are unclear for many GPCR families, including the bitter taste receptors (TAS2Rs). We ascertained TAS2R5 properties by live cell-based functional assays, direct binding affinity measurements using optical resonators, and atomistic molecular dynamics simulations. We focus on three agonists that exhibit a wide range of signal transduction in cells despite comparable ligand–receptor binding energies derived from direct experiment and computation. Metadynamics simulations revealed that the critical barrier to activation is ligand-induced opening of the G protein between the α-helical (AH) and Ras-like domains of Gα subunit from a precoupled TAS2R5-G protein state to the fully activated state. A moderate agonist opens the AH-Ras cleft from 22 Å to 31 Å with an energy gain of −4.8 kcal mol^{-1}, making GDP water-exposed for signaling. A high-potency agonist had an energy gain of −11.1 kcal mol^{-1}. The low-potency agonist is also exothermic for Gα opening, but with an energy gain of only −1.4 kcal mol^{-1}. This demonstrates that TAS2R5 agonist-bound functional potencies are derived from energy gains in the transition from a precoupled complex at the level of Gα opening. Our experimental and computational study provides insights into the activation mechanism of signal transduction that provide a basis for rational design of new drugs.

G protein-coupled receptor | bitter taste receptor | airway smooth muscle | FLOWER | metadynamics

Significance

Our study reveals the underlying molecular mechanisms of ligand-induced activation in the human bitter taste receptor TAS2R5. Despite similar binding energies, significant variations in agonist potencies were observed. Using live cell-based assays, optical resonators, and molecular dynamics simulations, we found that the activation energy of the opening of the Gα subunit for GDP–GTP exchange, rather than binding affinity alone, correlates highly with agonist potency. This finding refines our understanding of G protein-coupled receptor (GPCR) activation, paving the way for the rational design of new therapeutic agents targeting these receptors.

The G protein-coupled receptor (GPCR) family forms the largest group of membrane proteins in eukaryotic organisms, playing a crucial role in detecting and responding to external stimuli such as odorants, hormones, and neurotransmitters (1, 2). Over 800 GPCRs are expressed in humans and are responsible for regulating cellular responses in virtually every cell type and are adaptive or maladaptive in many diseases associated with metabolism, heart, lung, and vascular function, and the central nervous system; at least 30% of FDA-approved drugs target GPCRs (3, 4).

Binding of an extracellular agonist to an inactive GPCR stimulates multiple intracellular signaling pathways through conformational stabilization of the receptor which can lead to the activation of a heterotrimeric G protein composed of Gα, Gβ, and Gγ subunits (5). Upon activation, the guanosine diphosphate (GDP) in the Gα subunit is exchanged with guanosine triphosphate (GTP), resulting in the release of the Gα and Gβγ subunits to mediate downstream signaling. This "simple switch" scheme, whereby receptors jump from inactive to fully activated states has been shown to be inadequate to explain multiple aspects of in vitro or in vivo receptor responses to ligands (6–8). In contrast, multiple intermediate states of the receptor, from the inactive state to the agonist-bound, fully activated state, have been hypothesized or identified (6, 7, 9). These sequential structural states have the potential for differential interactions with the G protein along the transition, suggesting that they may be targeted to derive unique functional outcomes from ligand binding. Of note, in the context of this paper, these states refer to conformations that lead to G protein activation and no other signals such as those arising from receptor interaction with other partners (8, 10).

In our previous study for human bitter taste receptor subtype 5 (TAS2R5), we identified the binding site and binding poses for 1,10-phenanthroline (hereafter referred to as T5-1) and its 18 derivatives (T5-2 through T5-19) (10, 11). By focusing on the subtype-specific interactions, our predicted binding energies correlated well with experimental agonist–receptor signaling coefficients with R^2 = 0.851 for 14 agonists (*SI Appendix*, Fig. S1).

Author contributions: J.S., S.B.L., and W.A.G. designed research; M.Y.Y. performed computations; K.D.M. performed FLOWER experiments; H.R.S., S.A.H., and D.K. performed live cell experiments; M.Y.Y. and S.-K.K. analyzed computational results; and all authors discussed the results and wrote the paper.

Reviewers: M.D.V., Istituto Italiano di Tecnologia; and C.Z., University of Pittsburgh School of Medicine.

The authors declare no competing interest.

[1]M.Y.Y. and K.D.M. contributed equally to this work.

[2]To whom correspondence may be addressed. Email: judy@optics.arizona.edu, sliggett@usf.edu, or wag@caltech.edu.

This article contains supporting information online at https://www.pnas.org/lookup/suppl/doi:10.1073/pnas.2409987121/-/DCSupplemental.

Published November 20, 2024.

However, we noted 4 agonists that were outliers, with predicted strong interaction energies but displaying significantly lower receptor signaling activities measured by agonist-mediated increases in intracellular [Ca^{2+}] in intact cells. Such a discrepancy must be understood to establish structure–function relationships of TAS2Rs with respect to agonist activation needed both for development of therapeutic ligands and for understanding generalizable GPCR signaling mechanisms.

TAS2Rs, which are responsible for bitter taste perception, are considered to protect an organism from potentially toxic substances. TAS2Rs have been reported to be expressed in many extraoral tissues throughout the body (12, 13), including airway (14), gastrointestinal tract (15), heart (16), and brain (17). Many studies have reported that TAS2Rs are associated with various disorders and diseases, including asthma (18), cancer (19), and cardiovascular diseases (20), making TAS2Rs unique therapeutics targets. TAS2R5 is expressed in human airway smooth muscle cells, and agonists that act on TAS2R5 to relax these cells and relieve airflow obstruction are being considered for treatment of asthma and chronic obstructive pulmonary disease (COPD) (14, 21). TAS2Rs couple to the G_i family of G proteins, including gustducin in taste cells, and $G_{i1,2,3}$ in other cell types (21).

Herein, we employ both experimental and computational approaches to elucidate the molecular mechanisms underlying ligand-dependent signaling of TAS2R5 focusing on three agonists, T5-1 (moderate-potency), T5-8 (high-potency), and T5-14 (low-potency). Our experimental data in cellular assays reveal that these agonists exhibit significantly different potencies between T5-8 and T8-14, with a ~150-fold difference in EC_{50}. However, a method that directly measures ligand affinity using optical resonators (there are no radioligands) as well as binding energy calculations by molecular dynamics (MD) simulations exhibit similar binding affinities for T5-8 and T5-14 to the receptor. To resolve this discrepancy, we used metadynamics (metaD) simulations to predict the free energy surface for agonist-induced opening of the G protein in the precoupled TAS2R5-G protein complex to release the GDP held tightly in the G protein for release and signaling. Indeed, we find that the G protein opening for the outlier, T5-14, is substantially worse than the other agonists, T5-1 and T5-8, explaining its low potency. Thus, the signaling from the nonligand bound receptor to its G protein cannot necessarily be ascertained from agonist binding pocket energetics alone but requires an understanding of the GPCR-G protein as a complex leading to transmission of data to the cell interior via transducer activation. This appears to be particularly so for TAS2R agonists, where very few high-affinity agonists suitable for systemic administration have been found due to intrinsic low affinity and their proclivity to be activated by a large array of structurally diverse agonists.

Results

Functional Characteristics of T5-1, T5-8, and T5-14 in Live Cells. D9 cells that express TAS2R5 (14, 21) were studied as live cells, measuring agonist-stimulated increases in intracellular Ca^{2+} ($[Ca^{2+}]_i$), which represents the canonical pathway. The time-dependent $[Ca^{2+}]_i$ responses to the 3 compounds (Fig. 1 *A–C*) and the concentration–response curves normalized to the response to the nonspecific ionophore inonomycin (Fig. 1 *D–F*), respectively, reveal that each compound is an agonist. Mean responses from multiple experiments reveal a high potency for T5-8 and 150 times lower potency for T5-14. EC_{50} of T5-1 was 3-fold lower (i.e., greater potency) than that of T5-14 (Table 1). T5-14 also exhibited the lowest maximal response, consistent with it being a partial agonist. The calculated signal transduction coefficients (S.T.) (*Materials and Methods*) were consistent with T5-14 having the lowest transduction over baseline of the 3 agonists, with a rank order of T5-8 > T5-1 > T5-14.

FLOWER Toroid Functionalization and Receptor–Ligand Affinity Measurements. While the cell-based studies confirm that all three compounds are agonists, and by way of the EC_{50}s provide a potential rank order of the affinities, we pursued measurements of the true ligand–TAS2R5 binding affinity using the frequency locked optical whispering evanescent resonator (FLOWER) method (22, 23) (*Materials and Methods*). This method detects direct ligand–receptor binding regardless of the location of the interaction points, using receptors coated onto microtoroid resonators. FLOWER provides agonist–receptor interaction energies that should correlate with the computational predicted binding energies. The quality (Q)-factor which corresponds to

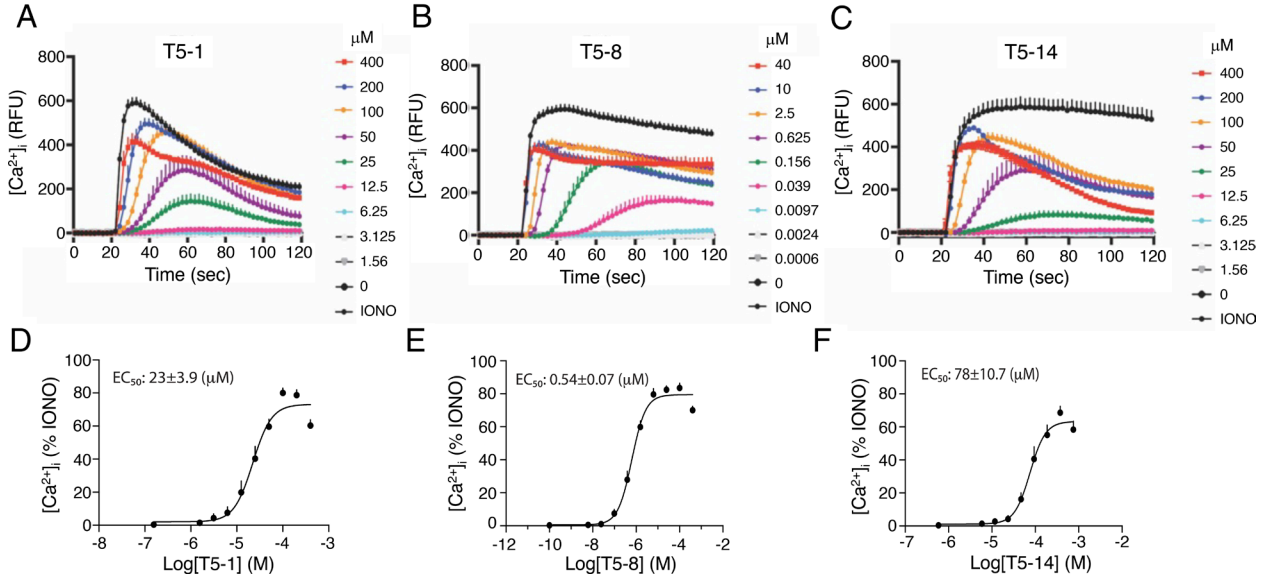

Fig. 1. D9 cells transfected to express TAS2R5 were plated in 96-well plates, loaded with Fluo-4AM, and exposed to the indicated concentrations of the agonists. The ionomycin (IONO) concentration was 2 μM. (*A–C*) are representative experiments showing the time-dependent increases in $[Ca^{2+}]_i$ from the indicated agonists. (*D–F*) are of mean data (normalized to the IONO response) fit to a sigmoid curve (n = 7 to 10). Table 1 for mean values of the EC_{50}, E_{Max}, and S.T coefficients.

Table 1. Summary of quantities obtained by experiments and simulations for three agonists

	Live cell Ca^{2+} measurements[†]				Flower[#]	Computation		
	EC_{50} (μM)[‡]	pEC_{50}	E_{max} (%IONO)[§]	S.T.[¶]	K_D (μM)	MD BE[‖] (kcal mol^{-1})	metaD DG (kcal mol^{-1})	*metaD* E_A (kcal mol^{-1})
T5-1	23.1 ± 3.99[*]	4.64	71.2 ± 2.41[*]	6.5	13 ± 3.5[*]	−32.6	−4.8	4.8
T5-8	0.54 ± 0.07	6.27	81.7 ± 2.37	8.2	0.9 ± 0.7	−41.9	−11.1	3.4
T5-14	78.4 ± 10.7[*]	4.11	63.7 ± 3.32[*]	5.9	2.5 ± 1.6	−41.5	−1.4	6.2
Apo	–	–	–	–	–	–	6.9	11.8

[*] $P < 0.05$ vs T5-8.
[†] Results are mean ± SE of 7 to 10 experiments.
[‡] EC_{50} is the concentration that achieves half-maximal response.
[§] E_{max} is the maximal $[Ca^{2+}]_i$ response to agonist minus baseline (no agonist), as a % of the ionomycin response.
[¶] S.T. is a log-transformed signal transduction coefficient (*Materials and Methods*).
[#] Results are mean ± SE of 3 experiments.
[‖] The calculated average binding energies from 3 replicas of 20 ns MD simulations (11).

photon lifetime of the toroid was calculated from the full-width half maximum (FWHM) of the resonance dip and was determined for each experiment to be ~10^5–10^6 (Fig. 2 *A* and *B*).

For T5-8 and T5-14, the estimated K_D values from FLOWER were 0.9 ± 0.7 μM and 2.5 ± 1.6 μM, respectively, while the K_D for T5-1 was 13 ± 3.5 μM (Fig. 2 *C*–*E* and Table 1). Thus, the direct binding of these agonists to the TAS2R5 showed a rank order of the K_Ds of T5-8 ~ T5-14 > T5-1. This places T5-14 with an affinity similar to T5-8, which differs substantially from the experimental functional results, where T5-8 is ~150-fold more potent than T5-14 and overall signal transduction is 2.3 orders of magnitude greater than T5-14.

Prediction of the Precoupled TAS2R5-G_i Protein Complex Structure. To understand the origin of the discrepancy between the measured binding affinities and the cell-based measurements of receptor activation by these agonists, we carried out computational approaches using MD and metaD simulations. Since there is no experimental structure for TAS2R5, we first used the well-equilibrated TAS2R5-agonist-G_i protein complex structure from our previous computational study (11). Briefly, we predicted the fully activated TAS2R5 by using the GPCR Ensemble of Structures embedded in Membrane BiLayer Environment (GEnSeMBLE) complete sampling methods that examines 13 trillion helix packings to determine 25 structures for docking (24, 25). We used DarwinDock complete sampling which examines 50,000 poses for each of the 25 TAS2R5 structures to select the best one (26). The G_i protein was then complexed to the receptor (forming ~12 new salt bridges between them), which was inserted into the lipid bilayer and followed by over 100 ns of MD simulations to equilibrate the full structure. We note that these calculations were carried out first for the fully activated ligand-TAS2R5-G_i protein structure.

To obtain the structure for the TAS2R5-G_i protein in the precoupled state prior to ligand binding, we first removed the agonist from the binding site and then replaced the activated G_i protein, which has a fully opened Gα subunit without GDP, with the inactive G_i protein containing GDP sandwiched between Ras-like and α-helical (AH) domains of the closed Gα subunit. This TAS2R5-G_i protein complex was inserted into the lipid bilayer with solvent at physiological salt and equilibrated over a 200 ns MD simulation (Fig. 3*A*). In this equilibrated TAS2R5-G_i protein structure, the terminal carboxylate of the Gα5 helix (GαF355) forms a salt bridge with $K106^{3.53}$ [the superscript is Ballesteros-Weinstein numbering (27), whereas in the fully activated system, GαF355 forms a salt

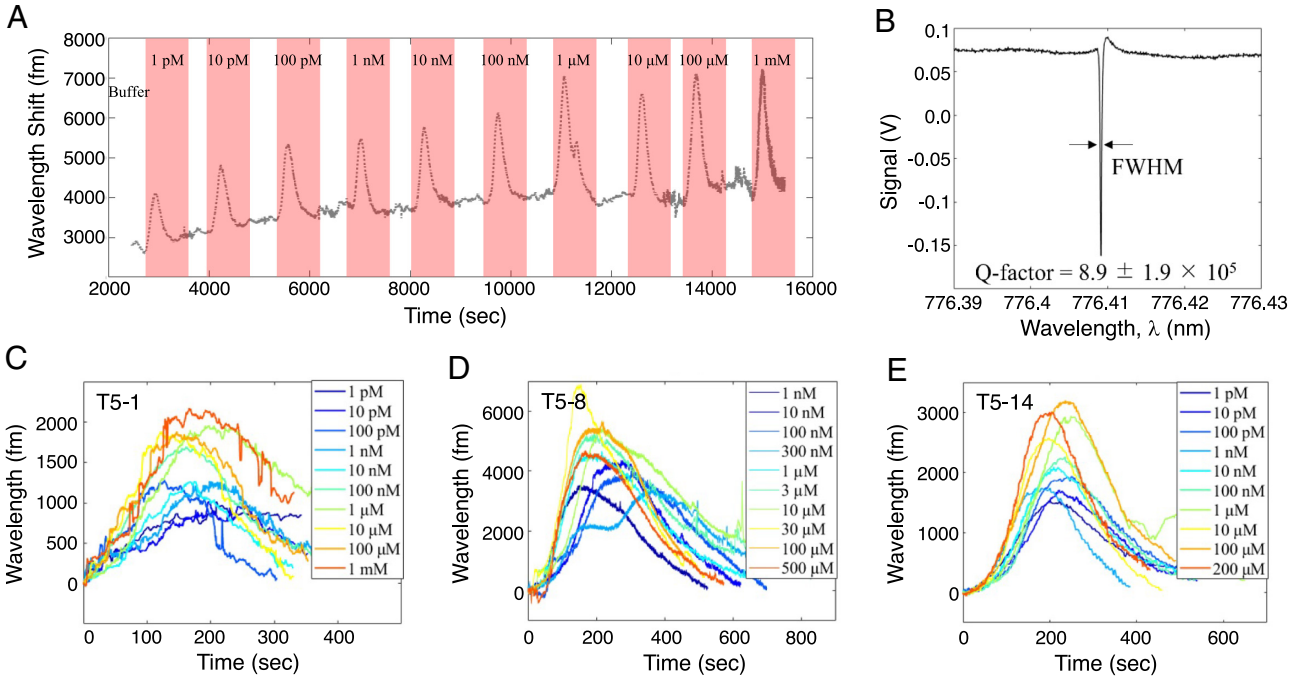

Fig. 2. The recorded signal from three different agonists binding to the TAS2R5 receptor. (*A*) The recorded binding signal in wavelength resonant shift over time for T5-14 binding to the TAS2R5 receptor, (*B*) a representative resonance dip. The Q-factor is calculated from the full-width half maximum (FWHM). (*C*–*E*) The wavelength shift response of each indicated agonist from representative experiments. Table 1 shows the mean K_D values from multiple experiments.

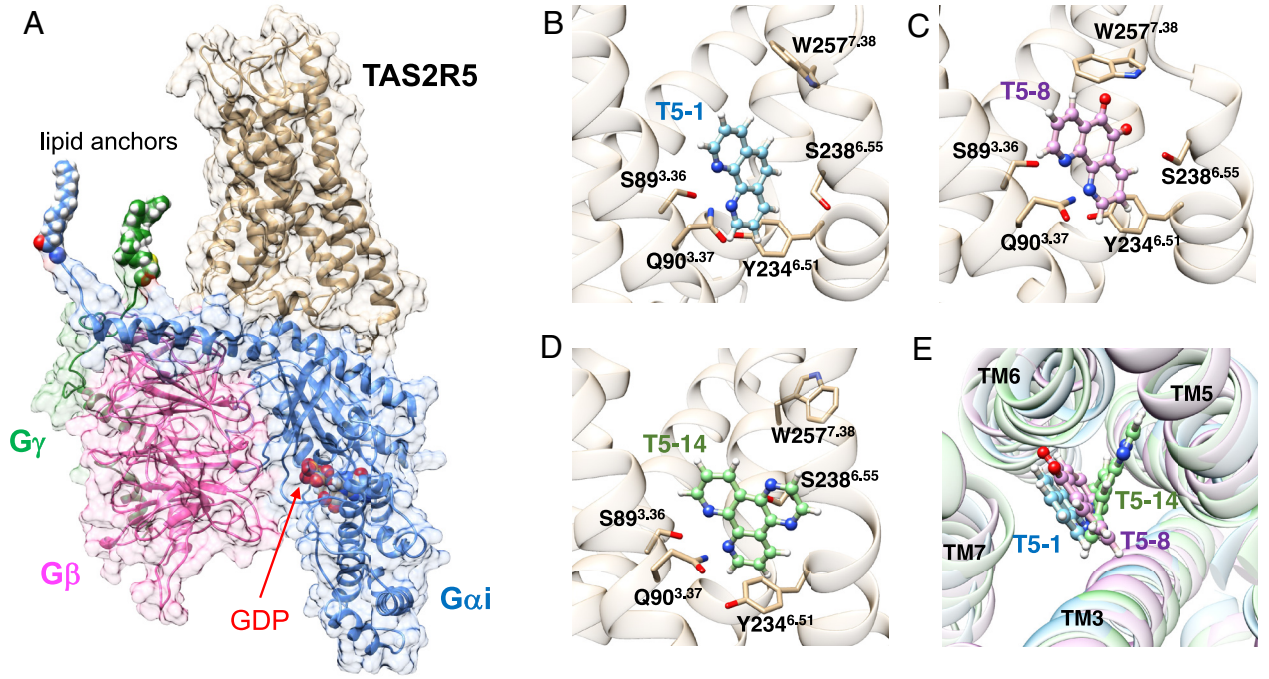

Fig. 3. (*A*) The equilibrated structure of the preactivated TAS2R5-G_i protein complex. (*B–D*) Binding sites of TAS2R5 with T5-1, T5-8, and T5-14, respectively (*Side* view). (*E*) Superimposed structures of three different agonists in the binding site (*Top* view).

bridge with K215$^{6.32}$ (*SI Appendix*, Fig. S2). Next, each of three ligands, T5-1, T5-8, and T8-14, was docked into the binding site and then equilibrated for over 150 ns (Fig. 3 *B–D*). In our previous study (11), we identified four key residues in the binding site, S89$^{3.36}$, Q90$^{3.37}$, S288$^{6.55}$, and W257$^{7.38}$. These TAS2R5-specific residues are important for ligand recognition and binding and are considered to provide subtype specificity to TAS2R5. In particular, the hydrogen bonds (HBs) of S89$^{3.36}$ and Q90$^{3.37}$ to the two nitrogen atoms at the inside of the ligands appear to provide key interactions for ligand recognition and high affinity. T5-8 containing two backside oxygen atoms is capable of forming additional HBs with S288$^{6.55}$ and W257$^{7.38}$, while T5-1 with no *o*-quinone makes HBs only with the residues in transmembrane helix 3 (TM3) (Fig. 3 *B* and *C*).

This difference results in significantly different binding energies between the ligand and the receptor, –32.64 ± 0.51 kcal mol^{-1} for T5-1 and –41.86 ± 0.91 kcal mol^{-1} for T5-8, respectively (11). Moreover, we consider the additional HBs of T5-8 with W257$^{7.38}$ to promote activation because the rotation of TM7 is one of the major structural changes upon activation (28, 29). These interactions of T5-8 with TM7 explain the experimentally observed large EC_{50} difference of T5-8 compared with the others.

T5-14 exhibits a binding energy similar to that of T5-8, –41.52 ± 0.63 kcal mol^{-1} (consistent with the similar experimental binding affinities from FLOWER experiments, see above). However, T5-14 showed a different position within the pocket (Fig. 3 *D* and *E*) (11) compared to T5-8 and T5-1. The large substituent of T5-14 causes a rotation of the ligand due to the limited size of the binding site, resulting in a different positioning within the pocket between the TM5 and TM6, instead of the TM6 and TM7 found for T5-8 and T5-1.

MetaD Simulations of the Transition from Precoupled to Activated TAS2R5. To understand how these difference in binding would affect downstream signaling, we conducted metaD simulations. MetaD is a technique used to enhance sampling in MD simulations, particularly when the energy barrier between states is too high to be overcome within a feasible simulation time. During a metaD simulation, a bias is incrementally applied to the potential energy surface for a set of predefined collective variables. As the simulation converges, the free energy surface is obtained by accounting for the applied bias potential throughout the simulation. We used these metaD simulations to evaluate the ligand-dependent energetics associated with the activation of the G_i protein from the precoupled state. For comparison, we also examined the apo protein with no ligand. We focused on the energetics (free energy difference, ΔG, and activation energies, ΔG^*) for opening between the AH domain (the center of mass of Cαs for residues 62 to 182) from the Ras-like domain (the center of mass of Cαs for residues 42 to 58, and 272 to 280 and 326 to 335), which defines the GDP binding site (Fig. 4 *A* and *B*). The results of the free energy calculations clearly show that agonists promote the opening of Gα subunit, while the apo protein cannot activate the G protein (Fig. 4 *C–F*). The moderate agonist, T5-1, shows the opening from 22 Å to 31 Å in the cleft between the AH and Ras-like domain with a free energy activation barrier of ΔG^* = 4.8 kcal mol^{-1} and an energy gain of ΔG = –4.8 kcal mol^{-1}, making GDP water exposed for exchange with GTP and signaling (Fig. 4*C*). This opening becomes more drastic for the high-potency agonist, T5-8, resulting in opening the cleft with a free energy activation barrier of ΔG^* = 3.4 kcal mol^{-1} and the energy gain of ΔG = –11.1 kcal mol^{-1} (Fig. 4*D*). The low-potency agonist, T5-14, also shows an exothermic process of Gα opening, but with a free energy activation barrier of ΔG^* = 6.2 kcal mol^{-1} and a small energy gain of ΔG = –1.4 kcal mol^{-1} (Fig. 4*E*). For all agonists, the standard MD simulations starting with the open state structure obtained from the metaD simulations show that it remains in the open state (*SI Appendix*, Fig. S4), which agrees with the estimated energetics by metaD simulations that the open state is more stable than that of the closed state. In comparison, opening the Gα subunit is endothermic for the apo protein with ΔG = 6.9 kcal mol^{-1} (Fig. 4*F*), indicating that the ligand binding is crucial to opening the Gα subunit to activate the system. The estimated free energy difference of Gα opening by metaD simulations

correlates very well with the experimentally obtained function-related quantities, such as pEC_{50} (R^2 = 0.98) or S.T. (R^2 = 0.99), compared to affinity measurements between the receptor and agonists (R^2 = 0.15 and 0.14, respectively) (*SI Appendix*, Fig. S5). The same poor correlation holds for the cell-based functional results with the computationally derived binding energies since the computations correlated with directly measured binding affinities to the isolated TAS2R5. Taken together, the rank order of the free-energy determinations for the transition is T5-8 > T5-1 > T5-14, which correlates with the functional cell-based studies.

Discussion

We utilized multiple experimental and computational methods to understand how agonists ultimately serve to initiate intracellular signaling with the chemosensory receptor TAS2R5. It has been difficult to devise a strategy for finding high-potency agonists for this receptor, since the family of TAS2Rs is known to exhibit low affinity for plant-based ligands and their analogs. Typical approaches have used molecular modeling at the presumed agonist binding pocket, with a calculation of binding energies, to rank compound leads. However, we found that this was insufficient to predict high-potency agonists, with clear outliers which have high apparent binding affinity from the computational methods (and FLOWER experiments), and reasonable efficacies, but nevertheless have low functional potencies (10, 11). Given that the computationally derived binding energies were confirmed by our direct ligand–receptor experiments using the optical resonators coated with partially purified receptors, we turned our attention to the energy of opening Gα to expose the GDP for exchange with GTP. These energies successfully predicted the measured agonist potencies. We note that other factors may influence the EC_{50} measured in cells, such as receptor expression levels, membrane composition, and kinetic on/off rates. Nevertheless, in our model cells, the experiments were conducted in parallel, with stable receptor expression, and the same time points for measuring $[Ca^{2+}]_i$ mobilization were utilized.

In a binary GPCR activation scheme, where the receptor is either "off" or "on", the agonist binding event is assumed to initiate and confer energy transfer to effectors, and thus, the energy of binding within the agonist-binding pocket would be a suitable measure of receptor activation. Instead, we show here that the GPCR forms a precoupled complex which is subsequently activated by binding of the agonist. Depending on the agonist and its binding site to this precoupled complex, the barrier to opening the Gα and signaling may be low with a very negative ΔG, as for our most active agonist T5-8, or the barrier may be higher with a less negative ΔG, as for our moderately active agonist T5-1, or the barrier may be even higher with a much less negative ΔG, as for our least active agonist, T5-14. It remains challenging to obtain information about the conformational dynamics of GPCRs traversing through these transition states, but as shown here, it is essential for predicting agonist functional activation since the calculation of the energy change between the precoupled and activated states correlates with function. Structure determination techniques such as X-ray crystallography and cryogenic electron microscopy (cryo-EM) typically enable capture of the lower energy states within an ensemble of conformations. Nevertheless, multiple transition states or intermediate conformations from biophysical techniques including cell assays (30), NMR (31), and fluorescence spectroscopy (32) have been reported. Such studies have indicated that ligands exhibiting different efficacies or potencies modulate the relative population of multiple conformational states (33–42) for several GPCRs, such as β_1-adrenergic receptor (β_1AR) (35), β_2AR (36), the adenosine A_{2A} receptor ($A2_{2A}$) (37), the μ-opioid receptor (μOR) (38), neurotensin receptor type 1 (NTSR1) (39, 40), and metabotropic $GABA_B$ receptor (41, 42).

Consistent with this mechanism derived, results from computational methods (23, 40, 42–44), experimental NMR (36) and fluorescence resonance energy transfer (45) have shown that agonists *alone* are not likely capable of stabilizing most receptors in their fully activated states. These studies suggest that G protein binding to promote a precoupled state may occur prior to agonist binding. In our work with multiple class A GPCRs, we found that G protein binding to form a precoupled complex occurs prior to agonist binding (42). Moreover, a recent cryo-EM study on TAS2R46 (46) determined the complex structure of the active receptor with $G_{s/gust}$ protein bound, but with the absence of any agonist (PDB ID: 7XP4 and 7XP5), supporting our conclusion on the formation of precoupled state prior to ligand binding. We find agonists with similar potencies can bind in various modes within the binding site depending on their structures, influencing distinct energetic changes being transmitted from the core of the receptor to the opening of the Gα subunit (Fig. 5). This is particularly so for the μ, κ, and δ-opioid receptors (47), 5-HT_{2T} and

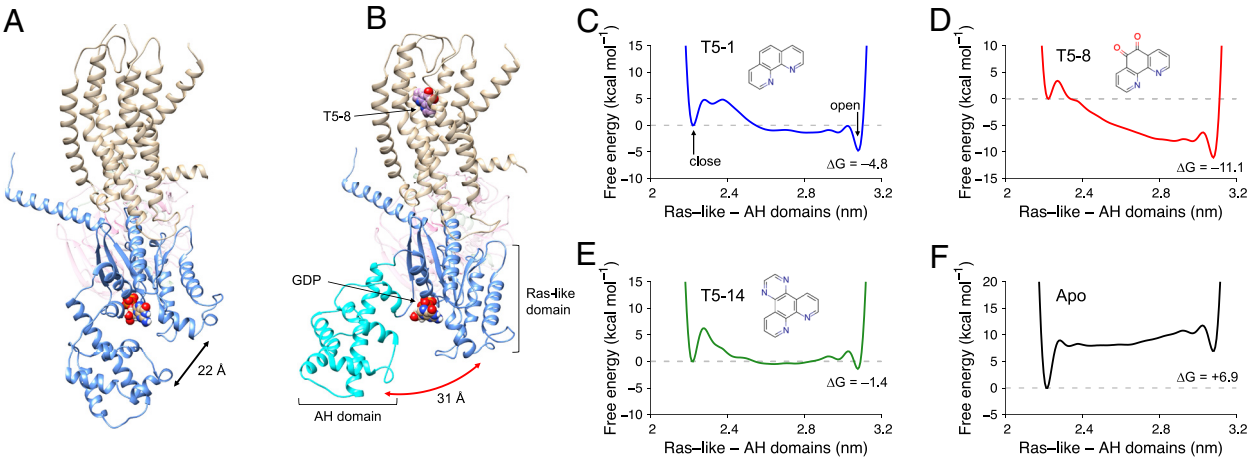

Fig. 4. Snapshot structures of metaD simulations for (*A*) apo and (*B*) T5-8-bound TAS2R5 representing closed and open conformations of Gα subunit, respectively. MetaD energetics associated with opening the Gα subunit as a function of the distance between the AH domain (the center of mass of Cαs for residues 62 to 182) from the Ras-like domain (the center of mass of Cαs for residues 42 to 58, and 272 to 280, and 326 to 335) for the TAS2R5-G_i protein with (*C*) T5-1 showing ΔG = −4.8 kcal/mol, (*D*) T5-8 showing ΔG = −11.1 kcal/mol, (*E*) T5-14 showing ΔG = −1.4 kcal/mol, and (*F*) apo showing ΔG = +6.9 kcal/mol.

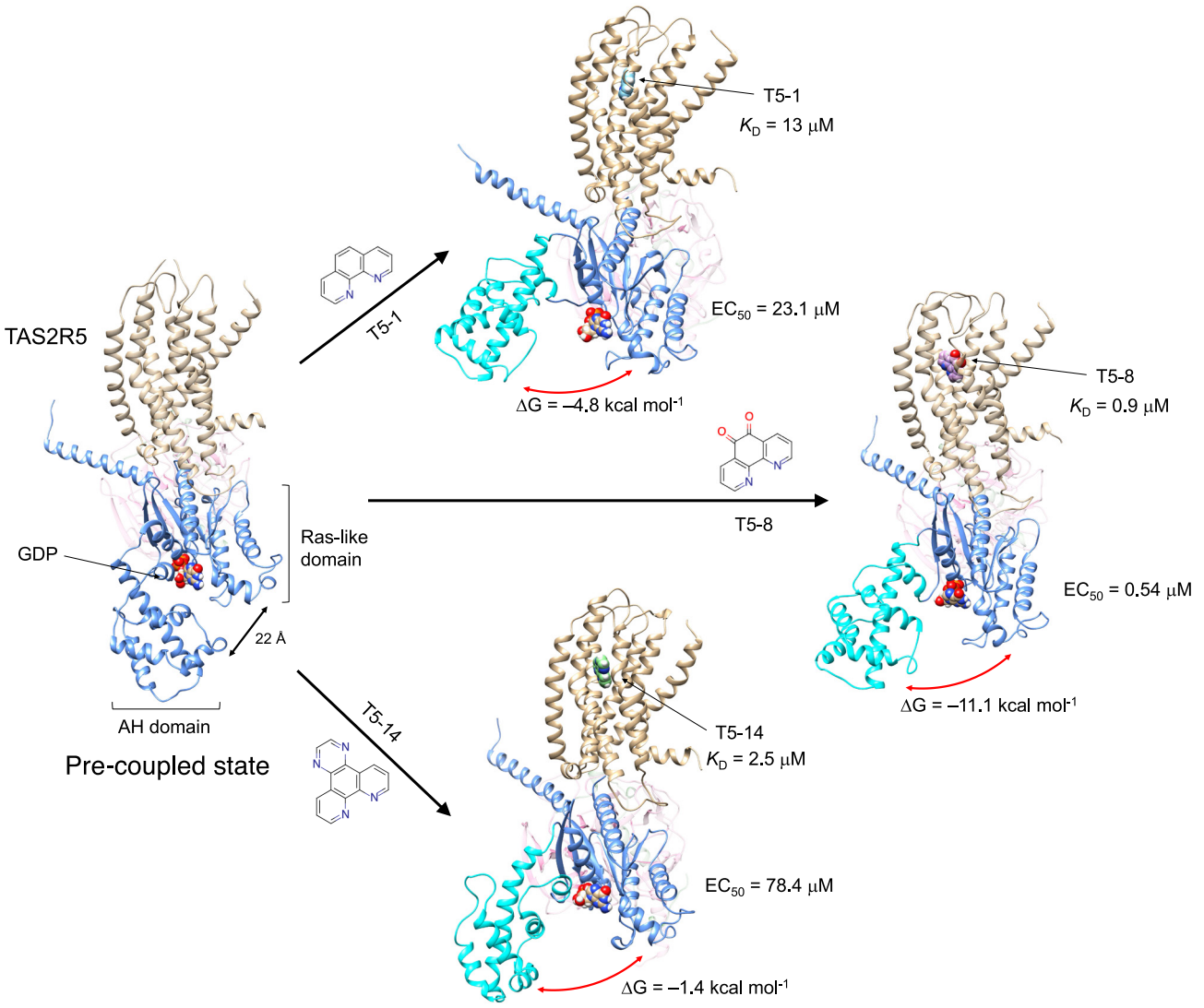

Fig. 5. Transitions from the precoupled state to the activated state induced by the binding of T5-1, T5-8, and T5-14, alongside the opening of Gα subunit. Agonist potencies correlate more strongly with the energetics of Gα subunit opening than with their binding affinities.

A_{2A} (43), and β_2AR (44), and now from the current work for TAS2R5. In some of our studies with other GPCRs, efficacy dependencies were more obvious than potency dependencies, but the net signal transduction, considering both attributes, is the critical characteristic for an effective agonist therapeutic.

For receptors such as TAS2Rs, which are ubiquitously expressed in multiple organs in the body showing promise as therapeutic targets, high-potency (<10 nM) full agonists have yet to be elucidated. In silico methods (13, 48–50) for ranking potential agonists for further study at a TAS2R may fail to identify useful compounds if only the binding energy is considered. Here, it is essential to examine how the potential agonist induces the precoupled GPCR-G protein complex to open to release GDP to induce signaling. This may be particularly important for TAS2Rs given the pharmacologic characteristics of the agonists known to date. Indeed, in our series of relatively similar compounds (derived from T5-1), computationally derived binding energies and measured affinities were insufficient for predicting functional potency. However, the free energy associated with the ligand induced transition from the GPCR-G protein precoupled state to the fully activated state correctly predicts agonist-promoted signaling of TAS2R5 to intracellular events.

Materials and Methods

Cells and Culture. An immortalized human airway smooth muscle cell line (D9) that expresses TAS2R5 (21) were grown in Dulbeccos Modified Eagle medium supplemented with 10% fetal bovine serum, 100 units/mL penicillin, and 100 μg/mL streptomycin at 37 °C in a 95% air 5% CO_2 atmosphere.

$[Ca^{2+}]_i$ measurements. D9 cells were plated at 10,000 cells per well in 96-well dishes and grown to 90% confluency overnight. They were loaded with Fluo-4 for 1 h at 37 °C in a 95% air 5% CO_2 atmosphere. The compounds were added, and fluorescence was read at 37 °C using a Flexstation 3 Multimodal Plate Reader (Molecular Devices). The peak response at each concentration was fit to a dose log transformed sigmoid curve using Prism (GraphPad, version 10.1.1), which provided the EC_{50} and the maximal response as a % of the IONO response (E_{Max}). The signal transduction coefficients were calculated as $\log(E_{Max}/EC_{50})$, with EC_{50} in Molar.

FLOWER. Affinity measurements were conducted using FLOWER (22, 23, 51–53). FLOWER is based on whispering gallery mode optical resonator technology (54, 55). Whispering gallery mode optical resonators are ultrasensitive biochemical sensors due to their long photon confinement times which enable increased light–matter interaction and thus high signal-to-noise biochemical sensing (53, 56–58). In these experiments, a microtoroid optical resonator was used. Changes in the environment surrounding the toroid leads to changes in its resonance

wavelength which is tracked (59) as a function of different concentrations of agonist that bind to the toroid's surface (22, 23, 60, 61). To determine the binding affinity of various agonists to the TAS2R5 receptor, we functionalized the toroid surface with TAS2R5 receptors which were expressed and extracted from HEK-293 cell membranes. The toroid was first incubated at 3 to 4 °C with DOPC (1,2-Dioleoyl-sn-glycero-3-phosphocholine) lipid vesicles for 1.5 h at a concentration of 0.5 mg/mL. This creates a layer of lipid vesicle on the toroid's surface. In parallel, the cell lysate was mixed with CellLyticM at a volumetric ratio of 1:3. The solution was then centrifuged at 12,500 rcf for 60 mins at 4 °C. Afterward, the supernatant which contains the TAS2R5 receptor was mixed with DBPS (phosphate-buffered saline, Dulbecco, pH = 7.4) at a volumetric ratio of 1:6 to reach a critical micelle concentration. The toroid was then incubated with this solution for 1.5 h. During this incubation, the TAS2R5 receptors will incorporate into vesicles on the surface of the toroid.

To find the K_D of each agonist to TAS2R5, varying concentrations of agonists were perfused over the toroid surface. Between each sample, a 5-minute buffer rinse was performed. The response signal from each concentration was analyzed based on the value of the peak response of the wavelength shift over time. This method of analysis is similar what is used for label-free dynamic mass redistribution (62, 63). The peak value corresponding to each concentration was then used to find the K_D value based on the following equation (64):

$$y = \frac{B_{\text{Max}} \times x^n}{x^n + {K_D}^n} + NS \times x + \text{background},$$

where y and x correspond to the response value and concentration value, respectively. B_{Max} is the maximum response of binding, n is the Hill coefficient, K_D is the binding affinity, NS is the nonspecific binding signal, and background represents the baseline signal.

Modeling the Precoupled TAS2R5-G_i Protein Complex. We began by using the well-equilibrated TAS2R5-agonist (T5-8)-G_i protein complex structure from our previous study (11). The TAS2R5-G_i protein in the precoupled state was obtained by a) removing the agonist from the binding site and b) replacing the activated G_i protein with the inactive G_i protein containing GDP sandwiched between Ras-like and AH domains of the closed Gα subunit. The constructed GPCR-G protein complex was embedded in a 1-palmitoyl-2-oleoyl-sn-glycero-3-phosphocholine (POPC) lipid bilayer consisting of 271 molecules within a ~100 × 100 × 140 Å^3 box. The final system contained ~150,000 atoms, including water molecules and a 100 mM concentration of sodium and chloride ions.

MD and metaD Simulations. All simulations were carried out with a 2 fs time step using GROMACS (65) with PLUMED (66). The CHARMM36m force field (67) was used, and the TIP3P model (68) was used to describe water molecules. The constructed system was first relaxed using steepest-descent energy minimization. The system was further equilibrated by performing NPT (constant number of particles, 1 bar pressure, and 310 K temperature) for 10 ns MD simulations, where positional restraints were placed on the heavy atoms with a force constant of 2.4 kcal mol^{-1} Å^{-2}. Then, a 200 ns NPT simulation on the TAS2R5-G_i protein structure was performed to fully relax the system and to prepare the preactivated state. Next, each of three agonists (T5-1, T5-8, and T8-14) were docked into the binding site and then equilibrated for over 150 ns.

Well-tempered metaD simulations were performed using PLUMED implemented in GROMACS (*SI Appendix*, Fig. S3). The bias forces were applied on the distance between the AH domain (the center of mass of Cαs for residues 62 to 182) from the Ras-like domain (the center of mass of Cαs for residues 42 to 58, and 272 to 280 and 326 to 335), which defines the GDP binding site in the Gα subunit. The bias was applied using a Gaussian width of 1.0 Å, an initial Gaussian height of 0.72 kcal mol^{-1}, a deposition interval of 1.0 ps, and a bias factor of 25. To preserve key interactions and prevent deformation of the helical secondary structure from artificial forces, the HBs between the agonists and the binding site residues and the distance between N(i + 4) and C(i) atoms within the Gα5 helix (residues 330 to 351) were restrained with a force constant of ~1.2 kcal mol^{-1} Å^{-2} during the metaD simulations. VMD (69) and Chimera (70) programs were used for analysis and visualization.

Data, Materials, and Software Availability. All study data are included in the article and/or *SI Appendix*.

ACKNOWLEDGMENTS. This work was funded by NIH grants R01HL155532 (S.B.L. and W.A.G.), P01HL114471 (S.B.L.), and R35GM137988 (J.S.).

Author affiliations: [a]Materials and Process Simulation Center, California Institute of Technology, Pasadena, CA 91125; [b]Department of Biomedical Engineering, The University of Arizona, Tucson, AZ 85721; [c]Department of Medicine, University of South Florida Morsani College of Medicine, Tampa, FL 33612; and [d]Department of Biomedical Engineering, Wyant College of Optical Sciences, The University of Arizona, Tucson, AZ 85721

1. R. J. Lefkowitz, Seven transmembrane receptors: Something old, something new. *Acta Physiol.* **190**, 9–19 (2007).
2. D. M. Rosenbaum, S. G. F. Rasmussen, B. K. Kobilka, The structure and function of G-protein-coupled receptors. *Nature* **459**, 356–363 (2009).
3. R. Santos *et al.*, A comprehensive map of molecular drug targets. *Nat. Rev. Drug Discov.* **16**, 19–34 (2017).
4. A. S. Hauser, M. M. Attwood, M. Rask-Andersen, H. B. Schiöth, D. E. Gloriam, Trends in GPCR drug discovery: New agents, targets and indications. *Nat. Rev. Drug Discov.* **16**, 829–842 (2017).
5. W. M. Oldham, H. E. Hamm, Heterotrimeric G protein activation by G-protein-coupled receptors. *Nat. Rev. Mol. Cell Biol.* **9**, 60–71 (2008).
6. S. Bockenhauer, A. Fürstenberg, X. J. Yao, B. K. Kobilka, W. E. Moerner, Conformational dynamics of single G protein-coupled receptors in solution. *J. Phys. Chem. B* **115**, 13328–13338 (2011).
7. R. Abrol, E. Serrano, L. Santiago, Development of enhanced conformational sampling methods to probe the activation landscape of GPCRs. *Adv. Protein Chem. Struct. Biol.* **128**, 325–359 (2022).
8. D. Kim *et al.*, Selective signal capture from multidimensional GPCR outputs with biased agonists: progress towards novel drug development. *Mol. Diagn. Ther.* **26**, 383–396 (2022).
9. J. Giraldo *et al.*, A 19F-qNMR-guided mathematical model for G protein-coupled receptor signaling. *Mol. Pharmacol.* **105**, 54–62 (2024).
10. D. Kim, S. S. An, H. Lam, J. W. Leahy, S. B. Liggett, Identification and characterization of novel bronchodilator agonists acting at human airway smooth muscle cell TAS2R5. *ACS Pharmacol. Transl. Sci.* **3**, 1069–1075 (2020).
11. M. Y. Yang, S.-K. Kim, D. Kim, S. B. Liggett, W. A. Goddard, Structures and agonist binding sites of bitter taste receptor TAS2R5 complexed with Gi protein and validated against experiment. *J. Phys. Chem. Lett.* **12**, 9293–9300 (2021).
12. I. Depoortere, Taste receptors of the gut: Emerging roles in health and disease. *Gut.* **63**, 179–190 (2014).
13. S.-J. Lee, I. Depoortere, H. Hatt, Therapeutic potential of ectopic olfactory and taste receptors. *Nat. Rev. Drug Discov.* **18**, 116–138 (2019).
14. D. A. Deshpande *et al.*, Bitter taste receptors on airway smooth muscle bronchodilate by localized calcium signaling and reverse obstruction. *Nat. Med.* **16**, 1299–1304 (2010).
15. S. V. Wu *et al.*, Expression of bitter taste receptors of the T2R family in the gastrointestinal tract and enteroendocrine STC-1 cells. *Proc. Natl. Acad. Sci. U.S.A.* **99**, 2392–2397 (2002).
16. S. R. Foster *et al.*, Bitter taste receptor agonists elicit G-protein-dependent negative inotropy in the murine heart. *FASEB J.* **28**, 4497–4508 (2014).
17. N. Singh, M. Vrontakis, F. Parkinson, P. Chelikani, Functional bitter taste receptors are expressed in brain cells. *Biochem. Biophys. Res. Commun.* **406**, 146–151 (2011).
18. S.-Y. Yoon *et al.*, Association between polymorphisms in bitter taste receptor genes and clinical features in korean asthmatics. *Respiration* **91**, 141–150 (2016).
19. L. T. P. Martin *et al.*, Bitter taste receptors are expressed in human epithelial ovarian and prostate cancers cells and noscapine stimulation impacts cell survival. *Mol. Cell Biochem.* **454**, 203–214 (2019).
20. D. Shiffman *et al.*, Association of gene variants with incident myocardial infarction in the cardiovascular health study. *Arterioscler. Thromb. Vasc. Biol.* **28**, 173–179 (2008).
21. K. Donghwa *et al.*, Coupling of airway smooth muscle bitter taste receptors to intracellular signaling and relaxation is via Gαi 1,2,3. *Am. J. Respir. Cell. Mol. Biol.* **56**, 716–726 (2017).
22. A. Gin *et al.*, Label-free, real-time monitoring of membrane binding events at zeptomolar concentrations using frequency-locked optical microresonators, *Nat. Commun.* **15**, 7445 (2024).
23. J. Su, A. F. Goldberg, B. M. Stoltz, Label-free detection of single nanoparticles and biological molecules using microtoroid optical resonators. *Light Sci. Appl.* **5**, e16001 (2016).
24. J. K. Bray, R. Abrol, W. A. Goddard, B. Trzaskowski, C. E. Scott, SuperBiHelix method for predicting the pleiotropic ensemble of G-protein–coupled receptor conformations. *Proc. Natl. Acad. Sci. U.S.A.* **111**, E72–E78 (2014).
25. M. Y. Yang, A. Mafi, S.-K. Kim, W. A. Goddard, B. Guthrie, Predicted structure of fully activated human bitter taste receptor TAS2R4 complexed with G protein and agonists. *QRB Discov.* **2**, e3 (2021).
26. A. R. Griffith, *DarwinDock & GAG-Dock: Methods and Applications For Small Molecule Docking* (California Institute of Technology, 2017).
27. J. A. Ballesteros, H. Weinstein, Integrated methods for the construction of three-dimensional models and computational probing of structure-function relations in G protein-coupled receptors. *Methods Neurosci.* **25**, 366–428 (1995).
28. J. A. Dalton, I. Lans, J. Giraldo, Quantifying conformational changes in GPCRs: Glimpse of a common functional mechanism. *BMC Bioinform.* **16**, 124 (2015).
29. J. J. Madsen, L. Ye, T. M. Frimurer, O. H. Olsen, Mechanistic basis of GPCR activation explored by ensemble refinement of crystallographic structures. *Prot. Sci.* **31**, e4456 (2022).
30. K. M. Small, S. L. Forbes, F. F. Rahman, S. B. Liggett, Fusion of β_2-adrenergic receptor to $G_{\alpha s}$ in mammalian cells: Identification of a specific signal transduction species not characteristic of constitutive activation or precoupling. *Biochem.* **39**, 2815–2821 (2000).
31. H. J. Kim, S. C. Howell, W. D. Van Horn, Y. H. Jeon, C. R. Sanders, Recent advances in the application of solution NMR spectroscopy to multi-span integral membrane proteins. *Prog. Nucl. Magn. Reson. Spectrosc.* **55**, 335–360 (2009).

32. H. Raghuraman, S. Chatterjee, A. Das, Site-directed fluorescence approaches for dynamic structural biology of membrane peptides and proteins. *Front. Mol. Biosci.* **6**, 96 (2019).
33. D. Hilger, The role of structural dynamics in GPCR-mediated signaling. *FEBS J.* **288**, 2461–2489 (2021).
34. D. P. Staus *et al.*, Allosteric nanobodies reveal the dynamic range and diverse mechanisms of G-protein-coupled receptor activation. *Nature* **535**, 448–452 (2016).
35. J. N. Frei *et al.*, Conformational plasticity of ligand-bound and ternary GPCR complexes studied by 19F NMR of the β1-adrenergic receptor. *Nat. Commun.* **11**, 669 (2020).
36. R. Nygaard *et al.*, The dynamic process of β2-adrenergic receptor activation. *Cell* **152**, 532–542 (2013).
37. L. Ye, N. Van Eps, M. Zimmer, O. P. Ernst, R. Scott Prosser, Activation of the A2A adenosine G-protein-coupled receptor by conformational selection. *Nature* **533**, 265–268 (2016).
38. R. Sounier *et al.*, Propagation of conformational changes during μ-opioid receptor activation. *Nature* **524**, 375–378 (2015).
39. H. E. Kato *et al.*, Conformational transitions of a neurotensin receptor 1–Gi1 complex. *Nature* **572**, 80–85 (2019).
40. I. Goba *et al.*, Probing the conformation states of neurotensin receptor 1 variants by NMR site-directed methyl labeling. *ChemBioChem* **22**, 139–146 (2021).
41. H. Shaye *et al.*, Structural basis of the activation of a metabotropic GABA receptor. *Nature* **584**, 298–303 (2020).
42. M. Y. Yang, S.-K. Kim, W. A. Goddard, G protein coupling and activation of the metabotropic $GABA_B$ heterodimer. *Nat. Commun.* **13**, 4612 (2022).
43. A. Mafi, S.-K. Kim, W. A. Goddard, The mechanism for ligand activation of the GPCR–G protein complex. *Proc. Natl. Acad. Sci. U.S.A.* **119**, e2110085119 (2022).
44. A. Mafi, S.-K. Kim, W. A. Goddard, The dynamics of agonist-β2-adrenergic receptor activation induced by binding of GDP-bound Gs protein. *Nat. Chem.* **15**, 1127–1137 (2023).
45. G. G. Gregorio *et al.*, Single-molecule analysis of ligand efficacy in β2AR–G-protein activation. *Nature* **547**, 68–73 (2017).
46. W. Xu *et al.*, Structural basis for strychnine activation of human bitter taste receptor TAS2R46. *Science* **377**, 1298–1304 (2022).
47. A. Mafi, S.-K. Kim, W. A. Goddard, The G protein-first activation mechanism of opioid receptors by Gi protein and agonists. *QRB Discov.* **2**, e9 (2021).
48. S. Basith *et al.*, Exploring G Protein-Coupled Receptors (GPCRs) Ligand space via cheminformatics approaches: Impact on rational drug design. *Front. Pharmacol.* **9**, 128 (2018).
49. D. Yang *et al.*, G protein-coupled receptors: Structure- and function-based drug discovery. *Sig. Transduct. Target. Ther.* **6**, 7 (2021).
50. A. T. N. Nguyen *et al.*, The application of artificial intelligence to accelerate G protein-coupled receptor drug discovery. *Br. J. Pharmacol.* **181**, 2371–2384 (2024).
51. J. Su, Label-free single molecule detection using microtoroid optical resonators. *J. Vis. Exp.* **106**, 53180 (2015).
52. G. T. Luu *et al.*, An integrated approach to protein discovery and detection from complex biofluids. *Mol. Cell. Proteomics* **22**, 100590 (2023).
53. C. Li *et al.*, Part-per-trillion trace selective gas detection using frequency locked whispering-gallery mode microtoroids. *ACS Appl. Mater. Interfaces* **14**, 42430–42440 (2022).
54. T. Lu, T.-T. J. Su, K. J. Vahala, S. E. Fraser, "Split frequency sensing methods and systems." US Patent 8,593,638 (2013).
55. C. Li, L. Chen, E. McLeod, J. Su, Dark mode plasmonic optical microcavity biochemical sensor. *Photon. Res.* **7**, 939 (2019).
56. Y. Xu *et al.*, Low part-per-trillion, humidity resistant detection of nitric oxide using microtoroid optical resonators. *ACS Appl. Mater. Interfaces* **16**, 5120–5128 (2024).
57. S.-K. Kim *et al.*, Methotrexate inhibits the binding of the severe acute respiratory syndrome coronavirus 2 (SARS-CoV-2) receptor binding domain to the host-cell angiotensin-converting enzyme-2 (ACE-2) receptor. *ACS Pharmacol. Transl. Sci.* **7**, 348–362 (2024).
58. S. Suebka, E. McLeod, J. Su, Ultra-high-Q free-space coupling to microtoroid resonators. *Light Sci. Appl.* **13**, 75 (2024).
59. S. Suebka, P.-D. Nguyen, A. Gin, J. Su, How fast it can stick: Visualizing flow delivery to microtoroid biosensors. *ACS Sens.* **6**, 2700–2708 (2021).
60. S. Suebka *et al.*, "Screening for effective COVID-19 drugs using microtoroid optical resonators" in *Conference on Lasers and Electro-Optics* (Optica Publishing Group, 2022), p. AM2I.5.
61. A. Gin, P.-D. Nguyen, E. Ozgur, J. Su, "Label-free ultrasensitive detection of amyloid-β using lipid-functionalized microtoroid optical resonators for early diagnosis of Alzheimer's disease" in *Biophotonics Congress: Optics in the Life Sciences Congress 2019 (BODA, BRAIN, NTM, OMA, OMP)*, (OSA, 2019), p. DW1B.5.
62. E. Tran, H. Sun, Y. Fang, Dynamic mass redistribution assays decode surface influence on signaling of endogenous purinergic P2Y receptors. *ASSAY Drug Dev. Technol.* **10**, 37–45 (2012).
63. L. Forster, S. Pockes, Investigating the ligand agonism and antagonism at the D2long receptor by dynamic mass redistribution. *Sci. Rep.* **12**, 9637 (2022).
64. H. J. Motulsky, R. R. Neubig, Analyzing binding data. *Curr. Protic. Neurosci.* **52**, 7.5.1–7.5.65 (2010).
65. M. J. Abraham *et al.*, GROMACS: High performance molecular simulations through multi-level parallelism from laptops to supercomputers. *SoftwareX* **1–2**, 19–25 (2015).
66. G. A. Tribello, M. Bonomi, D. Branduardi, C. Camilloni, G. Bussi, PLUMED 2: New feathers for an old bird. *Comput. Phys. Commun.* **185**, 604–613 (2014).
67. J. Huang *et al.*, CHARMM36m: An improved force field for folded and intrinsically disordered proteins. *Nat. Methods* **14**, 71–73 (2017).
68. W. L. Jorgensen, J. Chandrasekhar, J. D. Madura, R. W. Impey, M. L. Klein, Comparison of simple potential functions for simulating liquid water. *J. Chem. Phys.* **79**, 926–935 (1983).
69. W. Humphrey, A. Dalke, K. Schulten, VMD: Visual molecular dynamics. *J. Mol. Graph.* **14**, 33–38 (1996).
70. E. F. Pettersen *et al.*, UCSF Chimera–A visualization system for exploratory research and analysis. *J. Comput. Chem.* **25**, 1605–1612 (2004).